# Room Temperature Magnesium Electrodeposition from Glyme-Coordinated Ammonium Amide Electrolytes

AUTHOR(S):

Kitada, Atsushi; Kang, Yuu; Matsumoto, Kazuhiko; Fukami, Kazuhiro; Hagiwara, Rika; Murase, Kuniaki

CITATION:

Kitada, Atsushi ...[et al]. Room Temperature Magnesium Electrodeposition from Glyme-Coordinated Ammonium Amide Electrolytes. Journal of the Electrochemical Society 2015, 162(8): D389-D396

ISSUE DATE:

2015-05-02

URL:

http://hdl.handle.net/2433/201844

# Room Temperature Magnesium Electrodeposition from Glyme-Coordinated Ammonium Amide Electrolytes

**Atsushi Kitada,[a] Yuu Kang,[a] Kazuhiko Matsumoto,[b,*] Kazuhiro Fukami,[a,*] Rika Hagiwara,[b,*] and Kuniaki Murase[a,*,z]**

[a]*Department of Materials Science and Engineering, Kyoto University Kyoto 606-8501, Japan*
[b]*Graduate School of Energy Science, Kyoto University, Kyoto 606-8501, Japan*

We prepared less volatile and halide-free electrolytes for room temperature non-dendritic magnesium (Mg) electrodeposition by mixing a $Mg^{2+}$-amide-containing ionic liquid (IL) with equimolar glyme ($Mg^{2+}$+IL : glyme = 1:1). Raman spectroscopy suggested that in the equimolar mixture most glyme molecules are coordinated to $Mg^{2+}$ cations and/or IL cations, which is also supported by a single crystal X-ray diffraction study. The glyme-coordinated IL electrolytes showed sizable redox currents (order of mA $cm^{-2}$), while aging deterioration of electrochemical properties was observed for the triglyme mixture due to partial bath decomposition. The tetraglyme-coordinated IL electrolyte enabled flat electrodeposition of Mg with a metallic luster and showed with very high anodic stability (ca. +4 V vs. Mg) because of decrease in uncoordinated glymes, which can be used for high-voltage Mg ion batteries.
 [DOI: 10.1149/2.0731508jes] 

Manuscript submitted March 17, 2015; revised manuscript received May 11, 2015. Published June 3, 2015. This was Paper 65 presented at the Cancun, Mexico, Meeting of the Society, October 5–9, 2014.

In the last few decades elemental magnesium (Mg) has come to be viewed as one of the most interesting negative electrode materials for post lithium ion secondary batteries because of its high-theoretical capacity (3839 mAh $cm^{-3}$), low electrode potential (–2.356 V vs. SHE), and natural abundance. The well-known electrolytes for electrodepositing Mg metal at room temperature are Grignard electrolytes comprised of an ether solvent tetrahydrofuran (THF) and alkylmagnesium halides *R*Mg*X* (*R* = alkyl or aryl groups; *X* = Cl, Br). Addition of $AlCl_3$ makes more electroactive species of organo-halo-aluminates, giving larger current density and/or higher anodic stability.[1–10] However, the highly volatile THF and the highly moisture sensitive *R*Mg*X* and $AlCl_3$ are difficult to use practically. Safer alternatives to both solvents and solutes for Mg-ion battery electrolytes are still being sought.

Several groups have reported deposition of elemental Mg without using THF or *R*Mg*X*. Ionic liquids (ILs) are one of the least volatile solvents and efforts have been made to electrodeposit Mg from ILs. For example, Mg redox behavior has been observed in an IL solution of $Mg(ClO_4)_2$ or $MgCl_2$, although their current densities were significantly lower than those for *R*Mg*X*-dissolved ILs.[11] Some organic solvents that enable redox of Mg are less volatile than THF; these include 2-methyl-tetrahydrofuran,[12] and ethyleneglycol dimethylethers (glymes),[13–15] where Mg halides and hydrides were dissolved. Notably, glymes have boiling points above 150°C and are relatively safe at room temperature. However, in halide or hydride solutions hazardous halogen gas or hydrogen gas may evolve through anodic oxidation. From this viewpoint amide electrolytes are quite desirable as they hardly yield dissociated halogen ions.

Glyme solutions of magnesium amides such as bis[(trifluoromethyl)sulfonyl] amide $Mg(Tf_2N)_2$, where Tf denotes (trifluoromethyl)sulfonyl or $CF_3SO_2$, have recently been reported to show successful electrodeposition of Mg metal.[16–19] We have also reported an amide-containing glyme-IL solution with which room temperature electrodeposition of Mg metal was successfully demonstrated. In these $Mg^{2+}$-amide-containing glyme solutions, however, sizable amounts of free glyme molecules exists, as in IL-free glyme electrolytes, and thus all the reported electrolytes are either volatile and/or have limited anodic stability to some extent.

If free glymes were absent or decreased in an $Mg^{2+}$-containing electrolyte like in glyme-lithium salt equimolar complexes,[20] it would be a relatively safe electrolyte with lower vapor pressure and higher oxidative stability compared to the reported glyme-rich Mg amide solutions. Furthermore, we speculate that glymes can coordinate the ammonium cations of ILs since macrocyclic polyethers and open-chain polyethers can coordinate alkylammonium cations through hydrogen bonding,[21] and in fact no phase separation occurred in our previous study.[16] Therefore, it is of special interest to investigate glyme-based electrolytes where all glymes coordinate to any cations such as metal cations and/or ammonium cations of ILs. Notably, the reversible deposition/dissolution cycle of Mg was reported using $Mg^{2+}$-amide-containing ILs *without* glymes;[22–25] this was found to be highly suspicious in subsequent studies.[8,11,16,26–28]

In this paper, we studied the room temperature electrochemistry of metallic Mg using relatively safe electrolytes consisting of a $Mg(Tf_2N)_2$ and IL/glyme mixture. Addition of equimolar glyme to $Mg^{2+}$-containing ILs gave high stabilities toward oxidation of glymes, all of which seems to be coordinated to $Mg^{2+}$ or IL cations. Aging variation of electrochemical behaviors were observed, although the bulk properties of electrolytes were similar. Raman spectroscopy measurements suggested that the first coordination environment in solutions is comprised by oxygen atoms of glyme and of $Tf_2N^-$. Furthermore, galvanostatic electrolysis gave a thin and adherent film of elemental Mg with a metallic luster.

## Experimental

*Reagents.*— All reagents were used as received. Battery-grade $Mg(Tf_2N)_2$ was purchased from Kishida Kagaku. An ionic liquid PP13-$Tf_2N$ (*N*-methyl-*N*-propylpiperidinium bis[(trifluoromethyl) sulfonyl]amide) was purchased from Kanto Chemical. Electrochemistry-grade diethylene glycol dimethyl ether (diglyme; G2) was also received from Kanto Chemical. Ethylmagnesium bromide (EtMgBr) in THF (Kanto Chemical, 0.95 mol $dm^{-3}$) was used for electrolyte of the reference electrode (described later). Triethyleneglycol dimethyl ether (triglyme; G3) and tetraethyleneglycol dimethyl ether (tetraglyme; G4) were obtained from Tokyo Chemical Industry.

*Bath preparation.*— First, we made 0.5 mol $dm^{-3}$ $Mg(Tf_2N)_2$/PP13-$Tf_2N$ (molar ratio 1 : 7) by mixing at 80°C overnight under an inert atmosphere in a glove box. Then we mixed the IL solution with each glyme ($Mg(Tf_2N)_2$ : PP13-$Tf_2N$ : glyme = 1:7:8 by mole) with glass-coated stirrers for 30 min in a glove box to make 0.324 or 0.298 or 0.272 mol $dm^{-3}$ $Mg(Tf_2N)_2$ in IL/G2 or IL/G3 or IL/G4 solution. The water content of each bath was less than 50ppm, determined by Karl Fischer titration.

*Electrochemical Society Active Member.
zE-mail: murase.kuniaki.2n@kyoto-u.ac.jp

*Raman spectroscopy.*— Raman spectra were obtained at room temperature by an integrated Raman system (B&W Tek, innoRam 785) comprising a semiconductor laser light source (785 nm), a holographic probehead, an axial transmissive spectrograph, and a charge-coupled device (CCD) detector. The spectral acquisition time, i.e., exposure time of CCD and the number of exposures was varied for each sample so as to improve the signal-to-noise ratio of each spectrum.

*Bath properties.*— Conductivity measurements were performed at 25°C using a Radiometer Analytical CDM230. Viscosity measurements were conducted using SEKONIC VM-10A and VM-1G calibrated using a standard solution (NIPPON GREASE Co., Ltd.). The densities of the 0.5 mol $dm^{-3}$ $Mg^{2+}$-containing IL were calculated to be 1.46 g $cm^{-3}$ using the measured values of weight and volume, while those of glyme-mixed solutions were assumed to be 1.28 g $cm^{-3}$ for 0.324 mol $dm^{-3}$ $Mg(Tf_2N)_2$ in IL/G2 and 1.27 g $cm^{-3}$ for 0.298 mol $dm^{-3}$ $Mg(Tf_2N)_2$ in IL/G3 and 1.25 g $cm^{-3}$ for 0.272 mol $dm^{-3}$ $Mg(Tf_2N)_2$ in IL/G4 using the reported density of pure glymes (G2: 0.937 g $cm^{-3}$, G3: 0.986 g $cm^{-3}$, G4: 1.009 g $cm^{-3}$).

*Electrochemical properties.*— Electrochemical measurements were conducted in the glove box with a potentiostat/galvanostat (BAS, ALS ELECTROCHEMICAL ANALYZER 660C) at 30°C. Cyclic voltammetry (CV) was performed without stirring in an electrode cell of 20 $cm^3$ capacity with the planar dimension of WE fixed at 7.5 mmϕ (EC Frontier, VM-2A). Galvanostatic electrolysis was conducted using a glass cell of 15 $cm^3$ capacity with agitation speed of 300 rpm. Pt sheet and Mg sheet or rod (Nilaco, 99.9% purity) were used as the working electrode (WE) and counter electrode (CE), respectively. Because the potential of Mg was not stable in IL,[28] as reference electrodes (RE) we used a Mg rod immersed in EtMgBr in THF (0.95 mol $dm^{-3}$), separated from the main electrolyte by porous Vycor glass.[16] For measurements, Pt sheets were first washed with acetone and then with about 1 mol $dm^{-3}$ nitric acid before use. Mg sheets were polished with emery paper (#800) before measurements. In the potentiostatic electrolysis, WE and CE were arranged to be almost parallel.

*Characterization of electrodeposits.*— For characterizing the electrodeposits, X-ray diffraction (XRD) measurements and scanning electron microscope (SEM) observations were performed using RIGAKU RINT2200 and KEYENCE VE-7800, respectively.

*Single crystal growth of $Mg(Tf_2N)_2$-glyme complex.*— Battery-grade G2, G3, G4 and $Mg(Tf_2N)_2$ from Kishida Kagaku were used as reagents. Each glyme of 1.5 $cm^3$ and $Mg(Tf_2N)_2$ was mixed at a molar ratio of 3:1, heated to 90°C, and then slowly cooled to room temperature over 3 days. As a result, single crystals were successfully grown only from the G4 solution. The quality of crystals grown from the G2 solution was not sufficient to determine its crystal structure, and no single crystals were obtained from the G3 solution.

*Single crystal X-ray diffraction.*— Since the obtained glyme-$Mg^{2+}$-amide crystal was deliquescent, a white crystal with approximate dimensions 0.10 × 0.40 × 0.40 $mm^3$ was selected and transferred into a quartz capillary (0.5 mmϕ, dried under a vacuum at 150°C) under a dry Ar atmosphere, and centered on the X-ray diffractometer (R-axis Rapid II, Rigaku controlled by the program RAPID AUTO 2.40)[29] equipped with an imaging plate area detector and graphite-monochromatic Mo-Kα radiation (0.71073 Å). The end of capillary was filled with vacuum grease and then sealed using an oxygen burner. The measurement consisted of 20 ω scans (130–190°, 3°/frame) at the fixed φ (30°) and χ (45°) angles and 54 ω scans (0°–162°, 3°/frame) at the fixed φ (180°) and χ (45°) angles. Data collection was performed at −160°C with an exposure time of 450 s $deg^{-1}$. Integration, scaling and absorption corrections were performed using RAPID AUTO 2.40.[29] The structure was solved using SIR-92[30] and refined by SHELXL-97[31] linked to Win-GX.[32] Anisotropic displacement factors were introduced for all atoms except for hydrogen and hydrogen atoms, which were determined using an appropriate riding model.

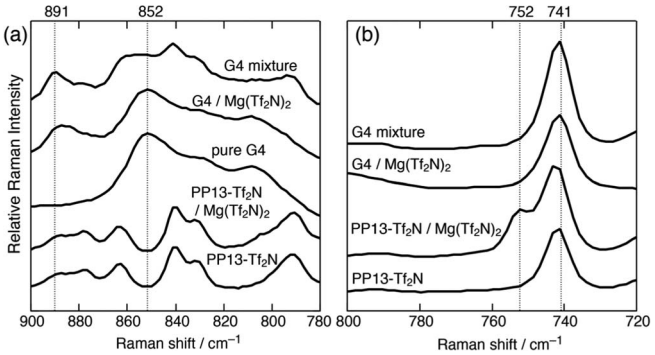


**Figure 1.** Raman spectra for the $Mg(Tf_2N)_2$:PP13-$Tf_2N$:G4 = 1:7:8 (mixture), $Mg(Tf_2N)_2$:PP13-$Tf_2N$ = 1:7, $Mg(Tf_2N)_2$:G4 = 1:8, pure G4, and PP13-$Tf_2N$: (a) obtained between 900 and 780 $cm^{-1}$ and (b) 800 and 720 $cm^{-1}$. Dashed lines emphasize specific peaks centered at 891, 852, 752, and 741 $cm^{-1}$.

## Results and Discussion

*Raman spectroscopy.*— In Raman spectroscopy the $CH_2$ rocking and C-O-C symmetric stretching vibration area ranged between 900 $cm^{-1}$ and 780 $cm^{-1}$. Figure 1 displays the Raman spectra for pure IL, pure G4, and G4 and/or IL solutions of $Mg(Tf_2N)_2$. It is known that C-O-C vibrations in ethers are usually seen in the regions between 890–850 $cm^{-1}$ on Raman measurements. In the case of free ethers, which are not coordinated by alkaline metal cations, the Raman band is observed at around 855 $cm^{-1}$.[33] Therefore, the Raman band at 852 $cm^{-1}$ is assignable to free G4, which is seen both in pure G4 and in G4 solution with $Mg^{2+}$:G4 = 1:8 by mole. The spectra for the IL/G4 mixture with $Mg^{2+}$:IL:G4 = 1:7:8 by mole can be viewed as a combination of the spectrum for Mg/G4 and that for Mg/IL. This takes into account that the profiles of Mg/IL and Mg/IL/G4 between 870 and 830 $cm^{-1}$ are quite similar except around 852 $cm^{-1}$. Since no phase separation was observed for the 1:7:8 mixed solution, the rest glymes should weakly coordinate IL cations through hydrogen bonding,[21] and the number of free (or uncoordinated) glymes should decrease. In the case of ethers coordinated by alkaline metal cations, the Raman band is seen at around 880 $cm^{-1}$ for mononuclear complex and at 890 $cm^{-1}$ for binuclear complex.[34,35] For $Mg^{2+}$, however, the binuclear complex would not exist due to high coulomb repulsive forces between the two $Mg^{2+}$. Therefore, we assign the band at 891 $cm^{-1}$ to mononuclear complex cations. The spectra for IL/G2 and IL/G3 resemble those for IL/G4 in appearance (see Fig. 2). Table I lists the vibrational frequencies of pure glyme and the Mg-glyme complex corresponding to the combination of $CH_2$ rocking and C-O-C stretching modes, the values of which are close regardless of glymes. Consequently, it is strongly indicated that sizable amount of glymes are coordinated to $Mg^{2+}$ cations in the 1:7:8 mixture.

In other spectrum regions, Raman spectra for $Tf_2N^-$ anions are specifically seen as $\delta(CF_3)$ vibration between 760 and 720 $cm^{-1}$.[36]

**Table I. Raman vibrational frequencies for each pure glyme and the Mg-glyme complex, corresponding to the combination of $CH_2$ rocking and C-O-C stretching modes.**

| Chemical species | Raman shift ($cm^{-1}$) |
|---|---|
| G2 | 854 |
| G3 | 852 |
| G4 | 852 |
| $[Mg(G2)_n]^{2+}$ | 889 |
| $[Mg(G3)_n]^{2+}$ | 885 |
| $[Mg(G4)_n]^{2+}$ | 891 |

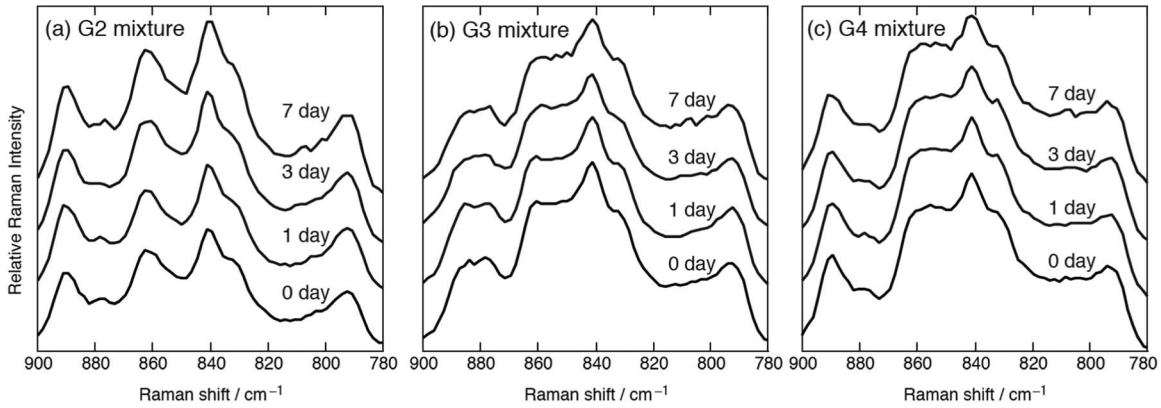


**Figure 2.** Raman spectra in the range of 900 $cm^{-1}$ and 780 $cm^{-1}$ for $Mg(Tf_2N)_2$:PP13-$Tf_2N$:glyme = 1:7:8, during 7 days after bath prepraration: (a) G2, (b) G3, and (c) G4 mixture. No aging variation was observed.

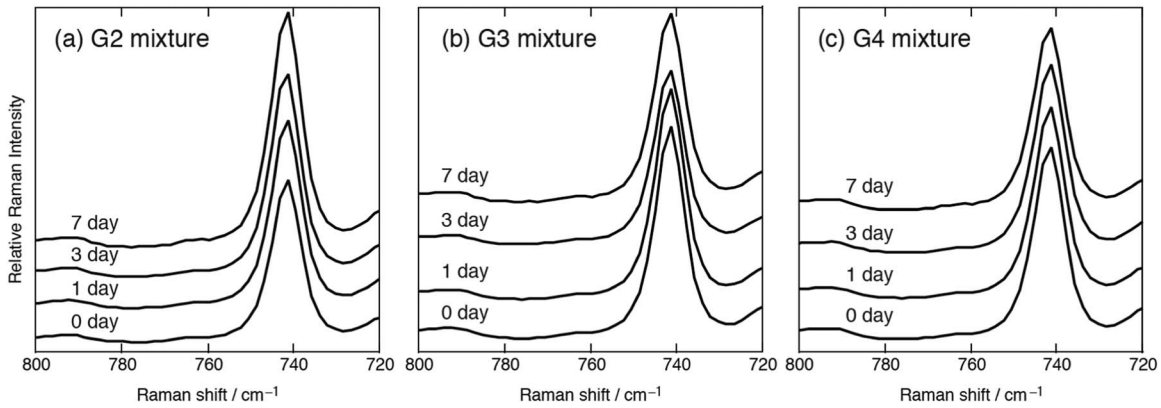


**Figure 3.** Raman spectra in the range of 800 $cm^{-1}$ and 720 $cm^{-1}$ for $Mg(Tf_2N)_2$:PP13-$Tf_2N$:glyme = 1:7:8, during 7 days after bath prepraration: (a) G2, (b) G3, and (c) G4 mixture. No aging variation was observed.

Figure 1b shows the Raman spectra obtained between 800 and 720 $cm^{-1}$. The Raman profile of the 1:7:8 Mg/IL/G4 mixture with a single peak centered at 741 $cm^{-1}$ is fairly similar to those of Mg-G4 and pure IL, which is different from that of $Mg^{2+}$-containing IL in that a shoulder peak was seen at 752 $cm^{-1}$ like the case of other divalent metal cations;[36] in a similar $Tf_2N$-based IL, metal(II) cations are coordinated by three $Tf_2N^-$ anions or six-O-coordinated complexes with the valence of –1. Thus we predict that without glymes $Mg^{2+}$ would exist in the form of $[Mg(Tf_2N)_3]^-$ in the IL solutions, while in the presence of glymes the coordination of $Tf_2N^-$ to $Mg^{2+}$ was significantly loosened and all $Tf_2N^-$ anions become free. The spectra in this range for IL/G2 and IL/G3 also resemble those for IL/G4 in appearance (see Fig. 3). Therefore, when glymes and ILs are mixed the coordination environment should change from $[Mg(Tf_2N)_3]^-$ to $[Mg(glyme)_n]^{2+}$. We also noted that within 7 days after bath preparation, there were no distinguishable changes in Raman spectra as displayed in Figs. 2 and 3.

*Single crystal structures of glyme-Mg($Tf_2N$)$_2$ complexes.*— Table II lists crystallographic data for the G4-$Mg(Tf_2N)_2$ complex. The fractional coordinates of each atom are listed in Table S1 (Supplemental Material). The crystal obtained from the 3:1 solution of G4 and $Mg(Tf_2N)_2$ crystallized into a monoclinic space group $P2_1/c$ and was found to be their 1:1 complex. While the $Li^+$ analogue of 1:1 complex of G4 and $LiTf_2N$ is liquid at room temperature,[20] the $Mg^{2+}$-complex was solid due to its relatively high charge density. Figure 4 shows the packing diagram of $[Mg(G4)](Tf_2N)_2$ structure viewed along the *b* axis. The structure is a quasi-two dimensional system, consisting of the Mg layer (represented by the blue Mg) with the G4 molecules and O atoms in the anion and fluorous layer (represented by green F). Figure 5 shows the coordination environment around $Mg^{2+}$. $Mg^{2+}$ was surrounded by five equatorial oxygen atoms of G4 and two axial oxygen atoms in two $Tf_2N^-$ anions to form a pentagonal bipyramid in $[Mg(G4)](Tf_2N)_2$. The observed glyme coordination in the solid form supports the Raman results from which we suggest the formation of $[Mg(glyme)]^{2+}$ in the glyme/IL solution. The equatorial oxygen atoms have longer Mg···O distances (2.1614(17)

**Table II. Crystallographic data for $[Mg(G4)](Tf_2N)_2$.**

| | |
|---|---|
| formula | $C_{14}H_{22}N_2O_{13}F_{12}MgS_4$ |
| fw | 806.89 |
| $T$ / K | 113 |
| cryst system | Monoclinic |
| space group | $P2_1/n$ |
| $a$ / Å | 10.1447(4) |
| $b$ / Å | 8.3961(3) |
| $c$ / Å | 35.3953(11) |
| β/° | 96.6300(10) |
| $V$ / Å$^3$ | 2994.67(18) |
| $Z$ | 4 |
| $\rho_{calc}$ / g $cm^{-3}$ | 1.790 |
| μ / $mm^{-1}$ | 0.474 |
| $R_1$[a] | 0.0392 |
| $wR_2$[b] | 0.0899 |
| cryst size / $mm^3$ | 0.10 × 0.40 × 0.40 |

[a] $R_1 = \Sigma||F_o| - |F_c||/\Sigma|F_o|$.
[b] $wR_2 = [\Sigma w(F_o^2 - F_c^2)^2/\Sigma w(F_o^2)^2]^{1/2}$.

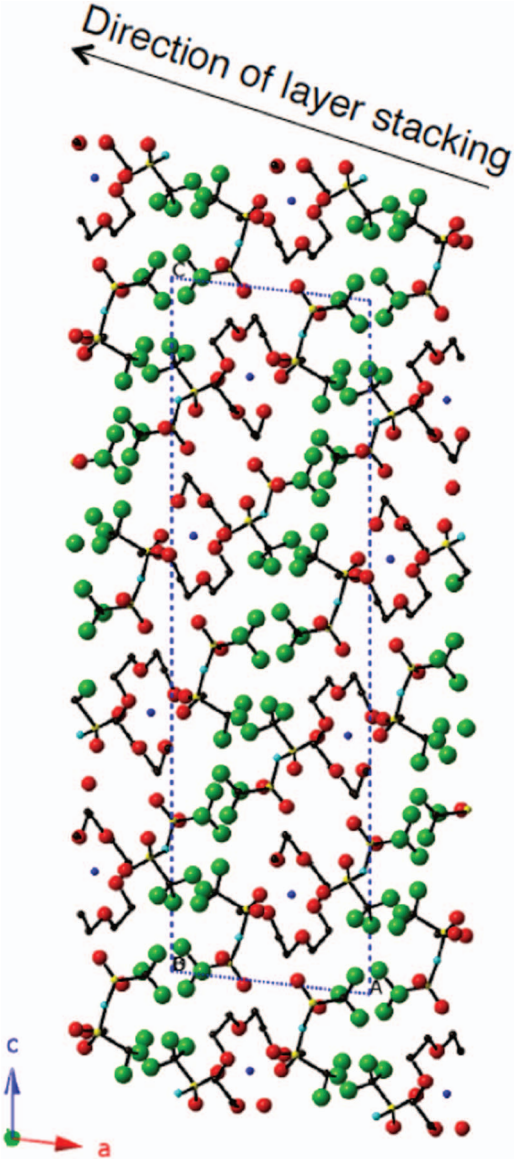


**Figure 4.** Schematic crystal structure of $[Mg(G4)](Tf_2N)_2$ viewed along the *b*-axis. Mg: blue, O: red, F: green, C: black, N: cyan, S: yellow. Hydrogen atoms are omitted for clarity. Unit cell is shown with blue dashed lines. The arrow shows direction of layer stacking.

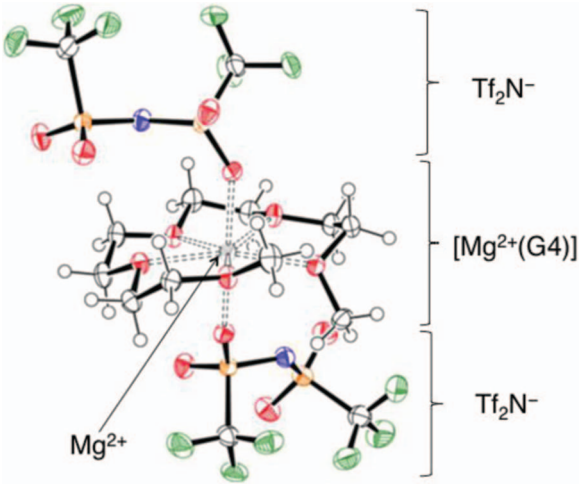


**Figure 5.** Coordination environment of Mg atom in $[Mg(G4)](Tf_2N)_2$ with ORTEP plot (50% thermal probability ellipsoids) of Mg (gray), O (red), C (white), S (orange), N (blue), F (green) with H (open spheres). Mg. . . O coordination is represented as dashed sticks, consisting of five equatorial oxygen atoms of tetraglyme and two axial oxygen atoms of two $Tf_2N^-$.

to 2.2402(17) Å) than those for the apical oxygen atoms (2.0385(17) and 2.0555(16) Å) (see Table S2, Supplemental Material), and thus the Mg ions have stronger interaction with the two $Tf_2N^-$ anions than with the G4 in solid, while in the solution $Mg^{2+}$ ions have less interaction with $Tf_2N^-$ as indicated by the Raman results. The bond valence ($v$) of each Mg···O interaction was calculated by the equation $v = \exp[(R_O–R)/B]$ ($R$ = Mg···O distance) using $R_O = 1.693$ and $B = 0.37$.[37] The bond valence sum of 2.00 for $Mg^{2+}$ in this structure is in excellent agreement with the ideal valence of 2+. This seven-coordination by oxygen atoms is in contrast to the five coordination for the lithium amide complex of G3 or G4, where one oxygen from $Tf_2N^-$ and four oxygen atoms from a glyme molecule coordinate.[38] The larger coordination number in the $Mg^{2+}$-complex comes from its stronger Lewis acidity than $Li^+$-complexes.

Considering that both the G3- and G4-$Li^+$ complexes have five-coordination of oxygen atoms, and that the bond valence sum of Mg in the G4-$Mg^{2+}$ complex closely matches the ideal valence, it can be deduced that other glyme-$Mg^{2+}$ complexes (G2 and G3) have the same coordination number. Given the seven oxygen coordination for Mg in the glyme amide complex and monodentate coordination of $Tf_2N^-$, one glyme (G2 or G3) and two $Tf_2N^-$ cannot donate seven oxygen ligands, and thus the number of conformation in the G2- or G3-$Mg(Tf_2N)_2$ complexes should be further increased compared to the G4 complex. This should be related to the fact that the G4 complex was obtained as a highly crystalline sample while the G2 complex was poorly crystalline and the G3 complex could not be obtained as a solid.

*Bath properties.*— Table III shows the conductivities and viscosities of $Mg(Tf_2N)_2$ solutions of PP13-$Tf_2N$-glyme mixture. As the molecular weight of glyme increased, the conductivities decreased and the viscosities increased monotonically. The viscosity of each glyme mixture is about 25–26 mPa s, one order of magnitude higher than that of the previously reported glyme-rich mixture (2.32 mPa s; $Mg^{2+}$:IL:G2 = 1:7:56 by mole).[16] However, the conductivities shown in Table III (2.6–3.8 mS $cm^{-1}$) are comparable to the previous values for glyme-rich mixtures (2.6 mS $cm^{-1}$ for $Mg^{2+}$:IL:G2 = 1:7:56, 2.52 mS $cm^{-1}$ for $Mg^{2+}$:G2 = 1:11, and 3 mS $cm^{-1}$ for $Mg^{2+}$:G3 = 1:7 by mole),[16,17,19] although slightly smaller than typical lithium-ion conductive electrolyte solutions. Notably, the bulk bath properties were fairly similar within 7 days for each IL/glyme mixture (see Fig. 6), which was consistent with the Raman results.

*Cyclic voltammetry.*— Figures 7a–7c shows the CVs for IL/glymes measured just after bath preparation. As shown in Fig. 7a, at –1.0 V vs. Mg the CV for G2 mixture showed sizable reduction currents up to about 6 mA $cm^{-2}$, 1.5 times larger than the previous report on diglyme-rich mixture.[16] Because the Mg complexes as cationic species in the solution which was revealed by the Raman results, they can more easily access the cathode surface due to the electrostatic attractions

**Table III. Molar ratio, molar concentrations, conductivities and viscosities of the glyme mixture with molar ratio of $Mg(Tf_2N)_2$:PP13-$Tf_2N$:glyme = 1:7:8 measured at 25°C 1 day after bath preparation.**

| Electrolyte | Concentration (mol $dm^{-3}$) | Conductivity (mS $cm^{-1}$) | Viscosity (mPa s) |
|---|---|---|---|
| G2 mixture | 0.324 | 3.8 | 25.2 |
| G3 mixture | 0.298 | 3.3 | 25.9 |
| G4 mixture | 0.272 | 2.6 | 26.0 |

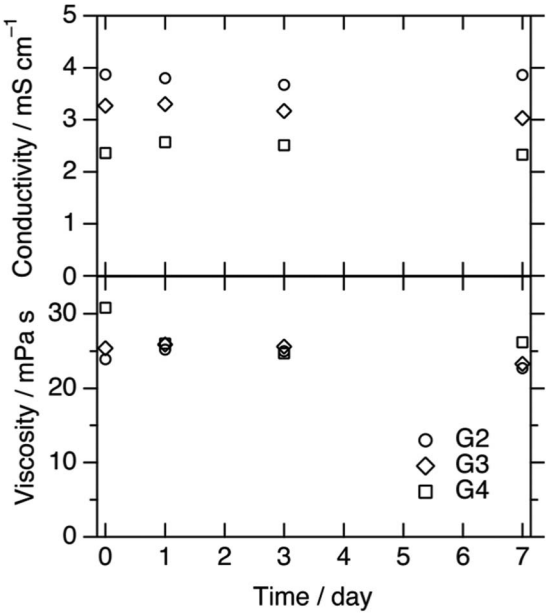


**Figure 6.** Conductivities and viscosities of the $Mg(Tf_2N)_2$:PP13-$Tf_2N$:G2 = 1:7:8, aged 0 day (within 1 h), 1 day, 3 days, and 7 days after bath preparation, showing that those values are independent of aging time.

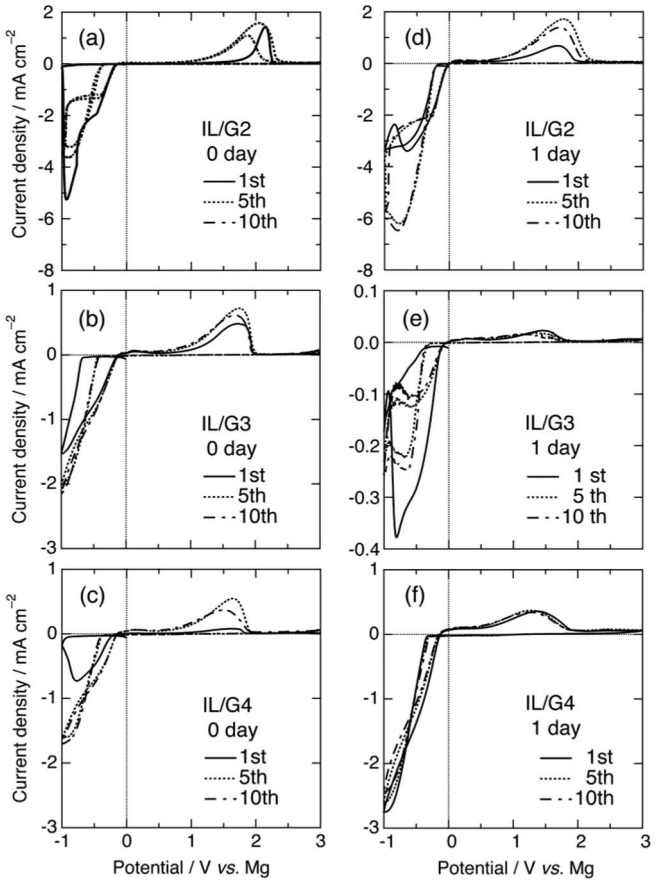


**Figure 7.** Cyclic voltammograms measured for the $Mg(Tf_2N)_2$-containing (a) PP13-$Tf_2N$/G2, (b) PP13-$Tf_2N$/G3, and (c) PP13-$Tf_2N$/G4 0 day (within 1 h) after bath preparation, and (d) PP13-$Tf_2N$/G2, (e) PP13-$Tf_2N$/G3, and (f) PP13-$Tf_2N$/G4 1 day after preparation. Aging variation was clearly seen for the G3 mixture. Sweep rate: 20 mV s$^{-1}$.

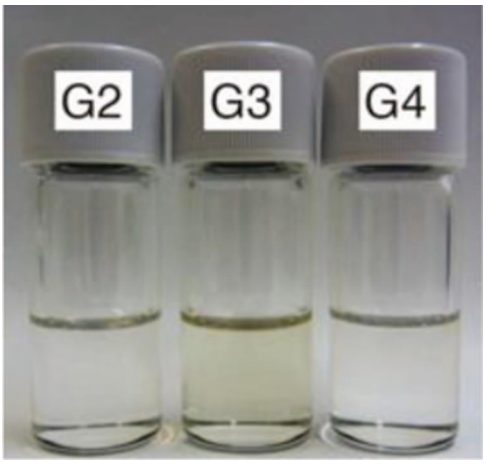


**Figure 8.** Photographs of the IL/glyme baths stored in a drybox for 7 days after preparation, where the IL/G3 mixture decomposed to became yellowish.

with cathode, giving the large current densities. Compared to the case of Ref. 16 the concentration of $Mg^{2+}$ is three times larger and the viscosity is about ten times larger while the conductivity is almost the same. Thus the present electrolyte has larger mobility of $Mg^{2+}$. By contrast, the redox currents for IL/G3 shown in Fig. 7b were five times smaller than those in 0.5 mol dm$^{-3}$ $Mg^{2+}$ in G3 solution.[19] Although the viscosity of the pure G3 solution is not presented, the viscosity can be one order of magnitude lower than the IL/G3 mixed solution, and both the concentration and conductivity are similar to those of the IL/G3. Thus similar mobility of $Mg^{2+}$ should be present in the pure G3 and the IL/G3 solutions.

Figures 7d–7f show CVs of the IL/glyme mixtures, aged for 1 day after mixing. Among them the G3 mixture has order-of-magnitude smaller redox currents than the others, while its bath properties are similar to the other glyme solutions. Without ILs, the G3 solution of $Mg(Tf_2N)_2$ shows as large current density as IL/G2 or IL/G4 mixture.[18,19] Moreover, the IL/G3 sample kept in a glove box for 7 days after mixing changed to yellowish from colorless while the others remained fairly colorless (see Fig. 8). Thus it is strongly indicated that the G3 mixture decomposed to some extent, affecting not its bulk properties (see Fig. 6) but its redox behavior. Consequently, among these $Mg^{2+}$-containing baths, PP13-$Tf_2N$/G4 showed relatively large reduction and oxidation currents and did not decay up to the 10th cycle (see Fig. 7f).

Regardless of the time since bath preparation, oxidation currents are clearly seen above +0.6 V vs. Mg. A similar anodic overpotential of 0.6 V has been reported in a pure G3 solution of $Mg(Tf_2N)_2$.[18,19] Dissolution of Mg is prohibited in these amide-based electrolytes because the $Tf_2N^-$ anions developed passivation films on the deposited Mg.[39–42]

*Anodic stability of IL/glyme mixtures.*— Figure 9 shows the linear sweep voltammogram of the Pt electrode obtained with a sweep rate of 1 mV s$^{-1}$. Comparison of Figs. 9a and 9b shows that aging variation was not seen except in the G2 mixture. The potentials for electrolyte decomposition were defined as the potential at which $i > 20$ μA cm$^{-2}$ was +3.70 V for the IL/G2, +3.95 V for the IL/G3, and above +4 V for the IL/G4 in Fig. 9b. According to the above definition, the decomposition potential of the 0.5 mol dm$^{-3}$ $Mg(Tf_2N)_2$/G3 solution locates at around +3.4 V vs. Mg QRE with the same sweep rate.[19] Such an improvement in anodic stability due to a lack of free glymes has also been reported in $LiTf_2N$/glyme solution.[20] Therefore, it is concluded that the IL/glyme mixtures have higher anodic stability than the IL-free $Mg(Tf_2N)_2$/G3 solution. It is also notable that as the number of ether oxygens increased the anodic stability

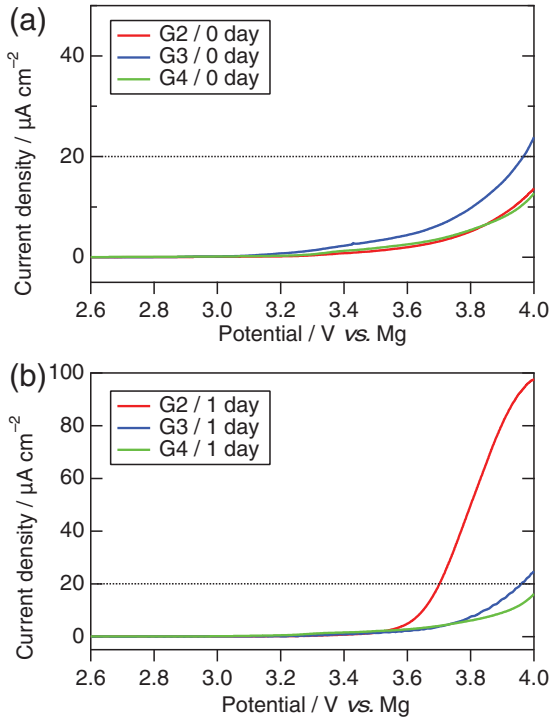


**Figure 9.** (color online) Linear sweep voltammograms of the Pt WE in the PP13-$Tf_2N$/glyme mixture: (a) 0 day (within 1 h) and (b) 1 day after bath preparation, showing high electrochemical stability toward oxidation.

became higher, due to the stronger chelating ability of the longer-chain polyethers.

*Electrolysis.*— As mentioned above, the IL/G4 mixture (aged 1 day) showed good redox behaviors and high anodic stability. In addition, G4 has higher boiling and flash points than G2 and G3, being attractive for practical use. Therefore we attempted electrodeposition of Mg metal from the PP13-$Tf_2N$/G4 mixture with cathodic current densities of 0.5, 1.5 and 2.5 mA $cm^{-2}$ up to 15 C. After galvanostatic electrodeposition at each current density electrodeposits were successfully obtained and their photographs, XRD patterns and SEM images are shown in Figs. 10–12. The XRD profiles of Pt WE shown in Fig. 11 confirmed that the electrodeposits consisted of elemental Mg without any sizable impurities. The SEM images of the Mg deposits shown in Fig. 12 demonstrate that all of their morphologies were not dendritic, in contrast to the case of Li with a typical dendritic morphology. Such dendrite-free Mg deposits have been obtained regardless of electrolytes.[16–19,43]

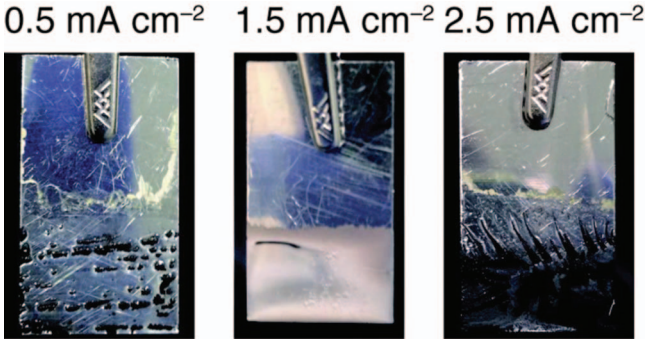


**Figure 10.** Photographs of the Pt substrates after cathodic electrodeposition at 0.5 mA $cm^{-2}$, 1.5 mA $cm^{-2}$, and 2.5 mA $cm^{-2}$ up to 15 C in the G4 mixture with a stirring speed of 300 rpm at 30°C.

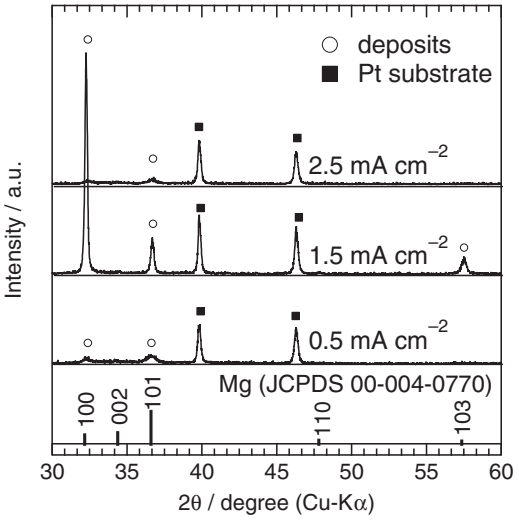


**Figure 11.** XRD profiles of the Pt substrates after the room-temperature electrodeposition at 0.5 mA $cm^{-2}$, 1.5 mA $cm^{-2}$, and 2.5 mA $cm^{-2}$, where the electrodeposits were identified as Mg metal.

The potential-time plots are shown in Fig. 13. Note that logarithmic scale is used on time axis. In the case of electrolysis at 1.5 mA $cm^{-2}$, the potential gradually increased from –0.8 V vs. Mg and became almost constant at –0.6 V within 10 s or 0.003 h. We suggest that the change in effective surface area is very little during electrolysis because nucleation of Mg crystal was accelerated at such a high current density. In fact, relatively flat electrodeposits with metallic luster were obtained (see Fig. 10), and the SEM image shows that Mg deposits were densely packed with relatively uniform grain size (2–5 μm; see Fig. 12b), because fine nuclei were largely produced. The current efficiency of electrodeposition at 1.5 mA $cm^{-2}$ was calculated to be about as high as 95.3% from the mass change of WE, although there were small deposits exfoliated from Pt WE.

The electrodeposition at 0.5 mA $cm^{-2}$ gave sparse deposits (see Fig. 10). We speculate that nucleation of Mg occurred at relatively low rate, which caused about an order-of-magnitude larger grain size than those obtained at 1.5 mA $cm^{-2}$ (see Fig. 12). In Fig. 13 the potential remained as low as –1.2 V vs. Mg for the first 0.001 h, due to electrolyte decomposition as well as Mg nucleation. The potential was followed by sudden increase to about –0.6 V and became almost constant, indicating that crystal growth became dominant rather than nucleus formation. The electrolysis at 2.5 mA $cm^{-2}$ was conducted at very low potentials ranging between –2.4 V and –1.8 V vs. Mg and the bath discolored to brown. This indicates sizable decomposition of electrolyte together with Mg electrodeposition, because the system is in diffusion-limited condition where Mg ion migration current was unable to catch up with the total current flowing the electrochemical cell.

In Fig. 11, taking into account that the intensities for Pt substrate are similar among the three XRD profiles, the peaks of deposits are very strong in the case of 1.5 mA $cm^{-2}$ while those at 0.5 and 2.5 mA $cm^{-2}$ are weak. Therefore, the observed XRD intensities are in good agreement with the cover area of Mg deposits. Besides, for electrodeposition using Grignard solutions, preferred orientation of {100} plane parallel to the substrate was observed only above 2 mA $cm^{-2}$.[43] By contrast, in each XRD pattern the intensity ratio of the 002 reflection was rather weak compared to the standard one even in the case of 0.5 mA $cm^{-2}$. Furthermore, for the galvanostatic electrodeposition at 0.5 mA $cm^{-2}$ in the IL-free 0.5 mol $dm^{-3}$ $Mg(Tf_2N)_2$ in G3 bath, the XRD pattern was quite similar to the standard one.[19] Thus it is suggested that the tendency to orient toward the {100} is more remarkable in the IL-containing baths.

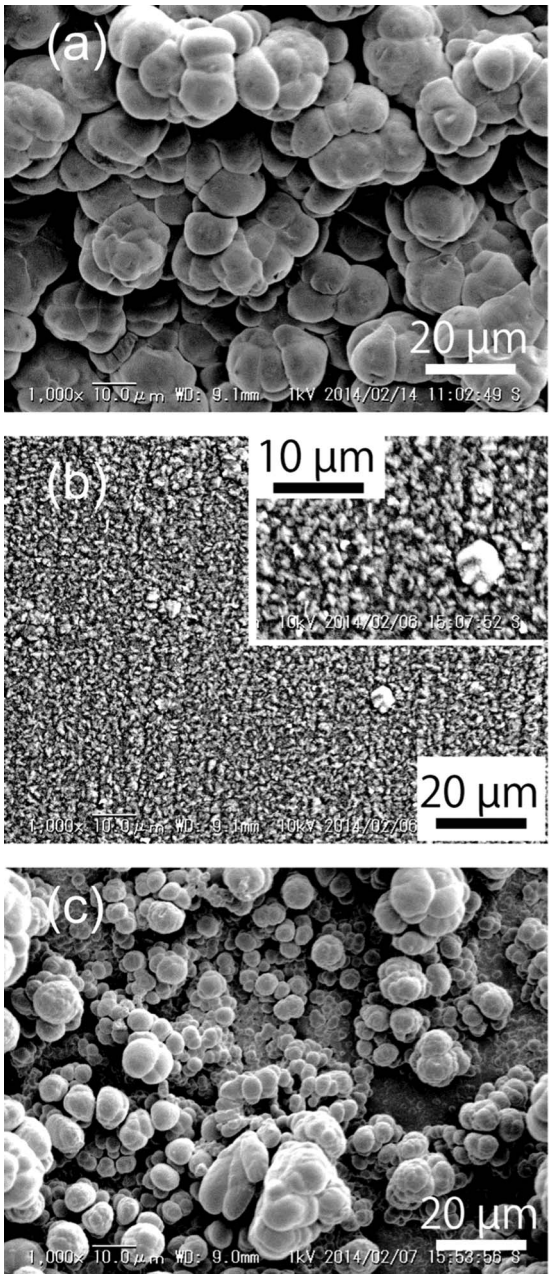


**Figure 12.** SEM images of the Mg electrodeposits obtained at (a) 0.5 mA $cm^{-2}$, (b) 1.5 mA $cm^{-2}$, and (c) 2.5 mA $cm^{-2}$, where no dendritic growth was observed.

## Conclusions

By mixing an $Mg(Tf_2N)_2$-containing IL with glyme solutions, we prepared a safe electrolyte without highly volatile solvents or free halide anions. We revealed that the equimolar mixture of glymes and $Mg^{2+}$-containing ILs caused a decrease in the number of free or uncoordinated glymes, which show sizable redox currents and high electrochemical stabilities toward oxidation. It was also indicated that $[Mg(glyme)_n]^{2+}$ cation is the Mg dissolved species in the IL/glyme mixture. Aging variation in electrochemical properties were observed especially for the triglyme solution, while the physicochemical properties (viscosity and conductivity) were almost unchanged. Flat electrodeposition of Mg metal with a metallic luster was demonstrated at room temperature using the PP13-$Tf_2N$/tetraglyme mixture. Although a large anodic overpotential for dissolving Mg metal is still observed, the glyme-coordinated amide-type-IL electrolytes may open-up new options for Mg-ion secondary battery electrolytes. Further studies on IL/glyme electrolytes with other mixing ratios are of special interest in terms of electrolyte improvements.

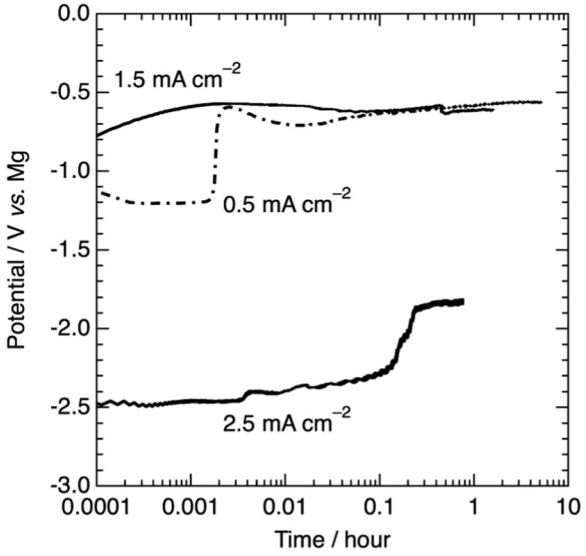


**Figure 13.** Potential-time plots for the electrodeposition at 0.5 mA $cm^{-2}$, 1.5 mA $cm^{-2}$, and 2.5 mA $cm^{-2}$ up to 15 C, where sizable cathodic decomposition of the electrolyte was indicated in the case of 2.5 mA $cm^{-2}$.

## Acknowledgments

This work was supported by the Core Research for Evolutional Science and Technology (CREST) program of the Japan Science and Technology Agency (JST). The work was also partly supported by Grant-in-Aid for Scientific Research (A) (No. 25249106) and Grant-in-Aid for Young Scientists (B) (No. 15K18253) from the Japan Society for the Promotion of Science (JSPS), and by the Kyoto University Global Frontier Project for Young Professionals (the John-Mung Advanced Program).

## References

1. C. Liebenow, *J. Appl. Electrochem.*, **27**, 221 (1997).
2. C. Liebenow, Z. Yang, and P. Lobitz, *Electrochem. Commun.*, **2**, 641 (2000).
3. D. Aurbach, A. Schechter, M. Moshkovich, and Y. Cohen, *J. Electrochem. Soc.*, **148**, A1004 (2001).
4. D. Aurbach, R. Turgeman, O. Chusid, and Y. Gofer, *Electrochem. Commun.*, **3**, 252 (2001).
5. Y. Viestfrid, M. D. Levi, Y. Gofer, and D. Aurbach, *J. Electroanal. Chem.*, **576**, 183 (2005).
6. Y. Gofer, O. Chusid, H. Gizbar, Y. Viestfrid, H. E. Gottlieb, V. Marks, and D. Aurbach, *Electrochem. Solid-State Lett.*, **9**, A257 (2006).
7. O. Mizrahi, N. Amir, E. Pollak, O. Chusid, V. Marks, H. Gottlieb, L. Larush, E. Zinigrad, and D. Aurbach, *J. Electrochem. Soc.*, **155**, A103 (2008).
8. N. Amir, Y. Vestfrid, O. Chusid, Y. Gofer, and D. Aurbach, *J. Power Sources*, **174**, 1234 (2007).
9. D. Aurbach, H. Gizbar, A. Schechter, O. Chusid, H. E. Gottlieb, Y. Gofer, and I. Goldberg, *J. Electrochem. Soc.*, **149**, A115 (2002).
10. H. S. Kim, T. S. Arthur, G. D. Allred, J. Zajicek, J. G. Newman, A. E. Rodnyansky, A. G. Oliver, W. C. Boggess, and J. Muldoon, *Nat. Commun.*, **2**, 427 (2011).
11. G. T. Cheek, W. E. O'Grady, S. Z El Abedin, E. M. Moustafa, and F. Endres, *J. Electrochem. Soc.*, **155**, D91 (2008).
12. M. Shiraga, F. Sagane, K. Miyazaki, T. Fukutsuka, T. Abe, K. Nishio, and Y. Uchimoto, Abstract 52, *The Electrochemical Society Meeting Abstracts*, Vol. 2010-02, Honolulu, USA, Oct 11, 2010.
13. R. E. Doe, R. Han, J. Hwang, A. J. Gmitter, I. Shterenberg, H. D. Yoo, N. Pour, and D. Aurbach, *Chem. Commun.*, **50**, 243 (2014).
14. R. Yasui, K. Asaka, K. Miyazaki, T. Fukutsuka, T. Abe, K. Nishio, and Y. Uchimoto, *Abstracts of the Electrochemical Society of Japan*, **80**, 238 (2013).
15. R. Mohtadi, M. Matsui, T. S. Arthur, and S.-J. Hwang, *Angew. Chem. Int. Ed.*, **51**, 9780 (2012).
16. A. Kitada, Y. Kang, Y. Uchimoto, and K. Murase, *J. Electrochem. Soc.*, **161**, D102 (2014).

17. S.-Y. Ha, Y.-W. Lee, S. W. Woo, B. Koo, J.-S. Kim, J. Cho, K. T. Lee, and N.-S. Choi, *ACS Appl. Mater. Interface*, **6**, 4063 (2014).
18. Y. Orikasa, T. Masese, Y. Koyama, T. Mori, M. Hattori, K. Yamamoto, T. Okado, Z.-D. Huang, T. Minato, C. Tassel, J. Kim, Y. Kobayashi, T. Abe, H. Kageyama, and Y. Uchimoto, *Sci. Rep.*, **4**, 5622 (2014).
19. T. Fukutsuka, K. Asaka, A. Inoo, R. Yasui, K. Miyazaki, T. Abe, K. Nishio, and Y. Uchimoto, *Chem. Lett.*, **43**, 1788 (2014).
20. K. Yoshida, M. Nakamura, Y. Kazue, N. Tachikawa, S. Tsuzuki, S. Seki, K. Dokko, and M. Watanabe, *J. Am. Chem. Soc.*, **133**, 13121 (2011).
21. E. P. Kyba, R. C. Helgeson, K. Madan, G. W. Gokel, T. L. Tarnowski, S. S. Moore, and D. J. Cram, *J. Am. Chem. Soc.*, **99**, 2564 (1977).
22. Y. NuLi, J. Yang, and R. Wu, *Electrochem. Commn.*, **7**, 1105 (2005).
23. Y. NuLi, J. Yang, J. Wang, J. Xu, and P. Wang, *Electrohem. Solid-State Lett.*, **8**, C166 (2005).
24. Y. NuLi, J. Yang, and P. Wang, *Appl. Surf. Sci.*, **252**, 8086 (2006).
25. Z. Feng, Y. NuLi, J. Wang, and J. Yang, *J. Electrochem. Soc.*, **153**, C689 (2006).
26. N. Yoshimoto, M. Matsumoto, M. Egashira, and M. Morita, *J. Power Sources*, **195**, 2096 (2010).
27. O. Shimamura, N. Yoshimoto, M. Matsumoto, M. Egashira, and M. Morita, *J. Power Sources*, **196**, 1586 (2011).
28. K. Murase, I. Sasaki, A. Kitada, Y. Uchimoto, T. Ichii, and H. Sugimura, *J. Electrochem. Soc.*, **160**, D453 (2011).
29. *RAPID AUTO*, version 2.40; Rigaku Corporation, Tokyo, Japan, 2006.
30. A. Altomare, G. Cascarano, C. Giacovazzo, and A. Guagliardi, *J. Appl. Crystallogr.*, **26**, 343 (1993).
31. G. M. Sheldrick, *SHELX-97*, University of Göttingen, Göttingen Germany, (1998).
32. L. J. Farrugia, *J. Appl. Crystallogr.*, **32**, 837 (1999).
33. T. Mandai, R. Nozawa, S. Tsuzuki, K. Yoshida, K. Ueno, K. Dokko, and M. Watanabe, *J. Phys. Chem. B*, **117**, 15072 (2013).
34. J. C. Lassègues, J. Grondin, and D. Talaga, *Phys. Chem. Chem. Phys.*, **8**, 5629 (2006).
35. J. Grondin, J. C. Lassègues, M. Chami, L. Servant, D. Talaga, and W. A. Henderson, *Phys. Chem. Chem. Phys.*, **6**, 4260 (2004).
36. K. Fujii, T. Nonaka, Y. Akimoto, Y. Umebayashi, and S. Ishiguro, *Anal. Sci.*, **24**, 1377 (2008).
37. I. D. Brown, *The Chemical Bond in Inorganic Chemistry: The Bond Valence Model*, Oxford University Press, Oxford, (2002).; the latest parameters are listed in http://www.iucr.org/resources/data/datasets/bond-valence-parameters.
38. T. Mandai, K. Yoshida, K. Ueno, K. Dokko, and M. Watanabe, *Phys. Chem. Chem. Phys.* **16**, 8761 (2014).
39. D. Aurbach, I. Weissman, Y. Gofer, and E. Levi, *Chem. Rec.*, **3**, 61 (2003).
40. M. Forsyth, P. C. Howlett, S. K. Tan, D. R. MacFarlane, and N. Birbilis, *Electrochem. Solid-State Lett.*, **9**, B52 (2006).
41. N. Birbilis, P. C. Howlett, D. R. MacFarlane, and M. Forsyth, *Surf. Coat. Technol.*, **201**, 4496 (2007).
42. M. Forsyth, W. C. Neil, P. C. Howlett, D. R. MacFarlane, B. R. W. Hinton, N. Rocher, T. F. Kemp, and M. E. Smith, *ACS Appl. Mater. Interfaces*, **1**, 1045 (2009).
43. M. Matsui, *J. Power Sources*, **196**, 7048 (2011).